Universality of Dzyaloshinskii-Moriya interaction effect over domain-wall creep and flow regimes

Duck-Ho Kim,[1,*] Dae-Yun Kim,[1,2] Sang-Cheol Yoo,[1,2] Byoung-Chul Min,[2] and Sug-Bong Choe[1,†]
[1]*Department of Physics and Institute of Applied Physics, Seoul National University, Seoul, 08826, Republic of Korea*
[2]*Center for Spintronics, Korea Institute of Science and Technology, Seoul, 02792, Republic of Korea*

(Received 23 November 2017; revised manuscript received 3 January 2019; published 1 April 2019)

Chirality causes diverse phenomena in nature such as the formation of biological molecules, antimatters, noncollinear spin structures, and magnetic skyrmions. The chirality in magnetic materials is often caused by the noncollinear exchange interaction, called the Dzyaloshinskii-Moriya interaction (DMI). The DMI produces topological spin alignments such as the magnetic skyrmions and chiral domain walls (DWs). In the chiral DWs, the DMI generates an effective magnetic field $\mu_0 H_{\mathrm{DMI}}$, resulting in a peculiar DW speed variation in the DW creep regime. However, the role of $\mu_0 H_{\mathrm{DMI}}$ over the different DW-dynamics regimes remains elusive, particularly due to recent observation of distinct behaviors between the creep and flow regimes. We hereby demonstrate experimentally that the role of $\mu_0 H_{\mathrm{DMI}}$ is invariant over the creep and flow regimes. In the experiments, the pure DMI effect is quantified by decomposing the symmetric and antisymmetric contributions of the DW motion. The results manifest that the antisymmetric contribution from chiral effect vanishes gradually across the creep and flow regimes, revealing that the symmetric contribution from $\mu_0 H_{\mathrm{DMI}}$ is unchanged. Though the DW dynamics is governed by distinct mechanisms, the present observation demonstrates the uniqueness of the DMI effect on the DWs over the creep and flow regimes, suggesting that the DMI-induced magnetic field is indeed a fundamental quantity of given magnetic systems.

DOI: 10.1103/PhysRevB.99.134401

I. INTRODUCTION

The Dzyaloshinskii-Moriya interaction (DMI) [1,2] has recently received considerable attention due to recent findings on the dynamics of magnetic chiral domain walls (DWs) [3–9]. Up until recently, Je *et al.* [10] demonstrated that, in the DW creep regime, the DMI-induced effective magnetic field $\mu_0 H_{\mathrm{DMI}}$ modifies the DW energy density and causes variation of the DW speed under the influence of an in-plane magnetic field $\mu_0 H_{\mathrm{in}}$. Such $\mu_0 H_{\mathrm{in}}$ dependence of the DW speed is found to be symmetric for inversion with respect to $\mu_0 H_{\mathrm{DMI}}$; thus, one can quantify the sign and magnitude of $\mu_0 H_{\mathrm{DMI}}$ by symmetry measurement of the DW speed with respect to $\mu_0 H_{\mathrm{in}}$ [10,11]. Recently, however, Jué *et al.* [12] proposed that energy dissipation—called chiral damping—generates additional variations of the DW speed, which is antisymmetric for inversion with respect to $\mu_0 H_{\mathrm{DMI}}$. Because of such sizeable antisymmetric contribution, the symmetry-based $\mu_0 H_{\mathrm{DMI}}$ determination becomes controversial in the DW creep regime. To avoid this controversial issue, Vaňatka *et al.* [13] demonstrated that in the flow regime, symmetry-based $\mu_0 H_{\mathrm{DMI}}$ determination becomes possible, as the flow regime exhibits symmetric DW speed variation, possibly due to the formation of soliton-like Bloch-type DWs above the Walker breakdown [14].

By developing this analysis scheme, we decompose the symmetric and antisymmetric contributions in the creep regime. This scheme is based on the fact that the symmetric and antisymmetric contributions exhibit distinct dependences on an out-of-plane magnetic field. The experimental results clearly show that the antisymmetric contribution gradually vanishes across the creep and flow regimes, while the symmetric contribution remains unchanged, confirming the uniqueness of $\mu_0 H_{\mathrm{DMI}}$ across the creep and flow regimes.

II. EXPERIMENTS & RESULTS

For this study, we chose 5.0-nm Ta/2.0-nm Pt/0.3-nm Co/2.0-nm Pt films with weak perpendicular magnetic anisotropy because of their high mobility of field-driven DW motion [15]. The domain images are observed by a magneto-optical Kerr effect microscope and then, the DW displacement is examined by capturing the DW images, where the out-of-plane magnetic field $\mu_0 H_z$ pulses are applied in the presence of in-plane magnetic field bias $\mu_0 H_x$. The field-driven DW speed v was then measured over a wide range from 5×10^{-4} to 20 m/s across the creep and flow regimes. Figure 1(a) plots v as a function of $\mu_0 H_z$ with $\mu_0 H_x = 0$ mT. The black arrow in the figure indicates the DW depinning field $\mu_0 H_{\mathrm{dep}}$, above which the DW exhibits a dissipative viscous motion with $v \propto \mu_0 (H_z - H_{\mathrm{dep}})$, as guided by the red line of the best linear fit. Therefore, this DW motion belongs to the flow regime ($\mu_0 H_z > \mu_0 H_{\mathrm{dep}}$). On the other hand, the creep regime ($\mu_0 H_z < \mu_0 H_{\mathrm{dep}}$) exhibits thermally activated DW motion with the creep criticality $\ln(v) \propto [\mu_0 H_z]^{-1/4}$, as guided by the blue line of the best linear fit in Fig. 1(b).

*Present address: Institute for Chemical Research, Kyoto University, Kyoto, 611-0011, Japan.
†Author to whom correspondence should be addressed: sugbong@snu.ac.kr

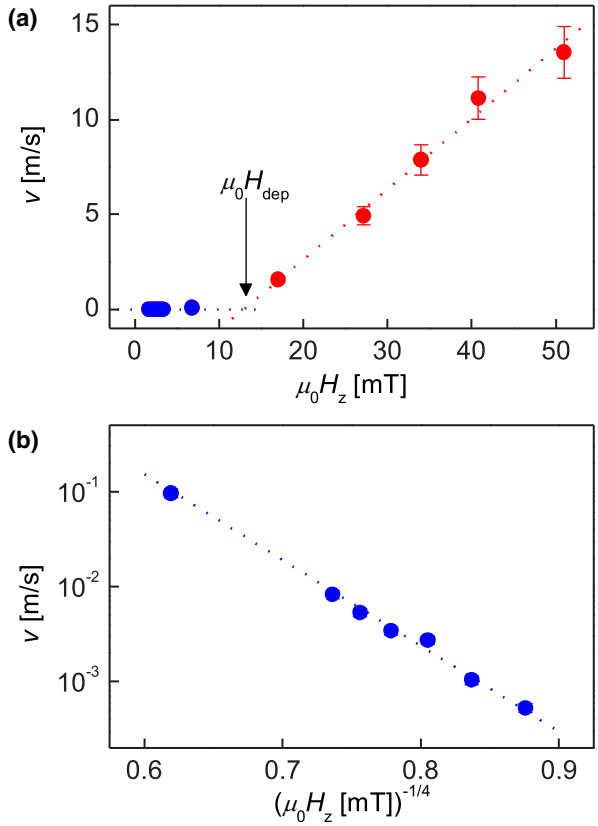

FIG. 1. Plot of v as a function of $\mu_0 H_z$ with $\mu_0 H_x = 0$. (a) Linear scale plot for the flow regime and (b) creep scale plot for the creep regime. The red line shows the best linear fit between v and $\mu_0 H_z$. The blue line shows the best linear fit between v and $[\mu_0 H_z]^{-1/4}$.

The effect of $\mu_0 H_x$ on the DW motion was then examined. Figures 2(a)–2(e) show $v/v_{\min}$ with respect to $\mu_0 H_x$ under various strengths of $\mu_0 H_z$, i.e., 1.9, 2.1, 3.4, 17, and 41 mT, respectively, over the creep and flow regimes. Here, $v_{\min}$ is the apparent minimum of v as defined below. The best parabolic fitting (solid curve) is shown in each plot to guide the symmetry of v, indicating the in-plane magnetic field $\mu_0 H_{\min}$ (purple arrows) for $v_{\min}$ [i.e., $v_{\min} \equiv v(\mu_0 H_{\min})$]. It is interesting to note that $\mu_0 H_{\min}$ is shifted across the plots with respect to the strength of $\mu_0 H_z$. Therefore, $\mu_0 H_{\min}$ of the creep regime (green dotted line) differs from that of the flow regime (blue dotted line). As the $\mu_0 H_{\mathrm{DMI}}$-determination scheme is based on the measurement of the inversion symmetry with respect to $\mu_0 H_{\min}$, this observation indicates that $\mu_0 H_{\mathrm{DMI}}$ cannot be uniquely determined irrespective of $\mu_0 H_z$. Because of better symmetries of $v(\mu_0 H_x)$ observed in the flow regime, Vaňatka *et al.* [13] have argued that $\mu_0 H_{\min}$ measured in the flow regime truly quantifies $\mu_0 H_{\mathrm{DMI}}$ $(=-\mu_0 H_{\min})$, whereas the asymmetric behavior in the creep regime contains sizeable antisymmetric contribution.

To confirm whether $\mu_0 H_{\min}$ measured in the flow regime corresponds to the true $\mu_0 H_{\mathrm{DMI}}$, we further analyze the DW motion in the creep regime by decomposing the symmetric and antisymmetric contributions. The principle of the decomposition is as follows: recent studies [10,15–17] have proposed that in the creep regime,

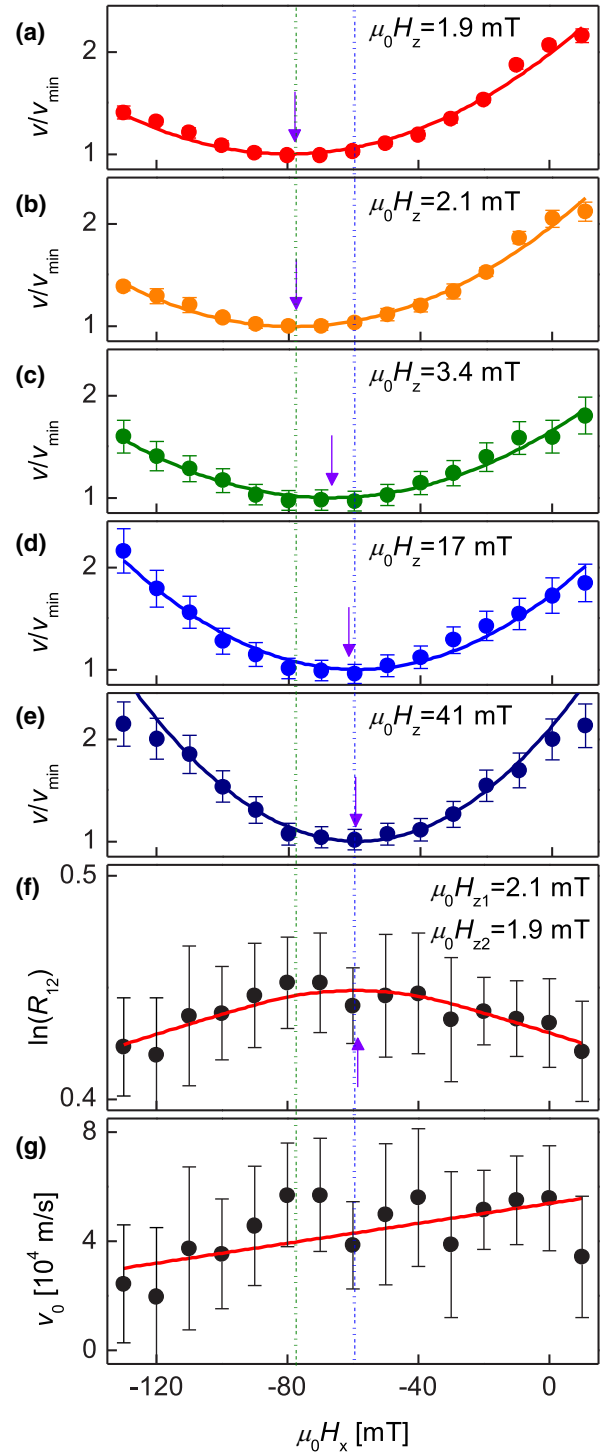

FIG. 2. Plot of $v/v_{\min}$ with respect to $\mu_0 H_x$ under various strengths of $\mu_0 H_z$: (a) 1.9, (b) 2.1, (c) 3.4, (d) 17, and (e) 41 mT. In each plot, the solid line shows the best parabolic fit with Eq. (9) and the purple arrow indicates $\mu_0 H_{\min}$ for $v_{\min}$. The DW speed is ranged (a) from 2.9×10^{-4} to 8.5×10^{-4}, (b) from 5.4×10^{-4} to 1.2×10^{-3}, (c) from 4.3×10^{-3} to 1.2×10^{-2}, (d) from $7.4 \times 10^{-1}$to 2.1, and (e) 4.8 to 13.8 m/s. The real scale of the DW speed is plotted in the Supplemental Material Fig. 2. (f) Plot of R_{12} with respect to $\mu_0 H_x$ with $\mu_0 H_{z1} = 2.1$ mT and $\mu_0 H_{z2} = 1.9$ mT. Here, $\ln[R_{12}] \equiv -\alpha(\mu_0 H_x)\{[\mu_0 H_{z1}]^{-1/4} - [\mu_0 H_{z2}]^{-1/4}\}$. The solid line shows the best fit with Eq. (5). (g) Plot of v_0 with respect to $\mu_0 H_x$. The solid line shows the best linear fit.

the thermally activated DW motion follows the DW creep criticality [18] as given by $v(\mu_0 H_x, \mu_0 H_z) = v_0(\mu_0 H_x) \exp[-\alpha(\mu_0 H_x)[\mu_0 H_z]^{-1/4}]$, where v_0 is the characteristic speed and α is a scaling parameter related to the energy. According to Ref. [10], $\alpha(\mu_0 H_x)$ mainly attributes the symmetric contribution by varying the DW energy density. On the other hand, it has been proposed in Ref. [12] that $v_0(\mu_0 H_x)$ possibly includes a sizeable antisymmetric contribution, even though the nature of $v_0(\mu_0 H_x)$ is not fully understood yet. The troublesome $v_0(\mu_0 H_x)$ can be easily removed experimentally by measuring two $v(\mu_0 H_x)$ under the influence of different out-of-magnetic field biases, $\mu_0 H_{z1}$ and $\mu_0 H_{z2}$ [19]. The ratio R_{12} of these two $v(\mu_0 H_x)$ is then written as

$$\ln[R_{12}(\mu_0 H_x)] = -\alpha(\mu_0 H_x)\left\{\left[\mu_0 H_{z1}\right]^{-1/4} - \left[\mu_0 H_{z2}\right]^{-1/4}\right\}, \tag{1}$$

which contains only the symmetric contribution from $\alpha(\mu_0 H_x)$. Figure 2(f) plots $R_{12}(\mu_0 H_x)$ with $\mu_0 H_{z1} = 2.1$ mT and $\mu_0 H_{z2} = 1.9$ mT. The black curve in the plot is the best fit to guide the symmetry of R_{12}. The equations and parameters for the best fit will be discussed later. The figure clearly shows that the inversion symmetry axis of $R_{12}(\mu_0 H_x)$ becomes identical to that (blue dotted line) of the flow regime. This observation, therefore, supports the claims that the inversion symmetry axis of the flow regime corresponds to the true $\mu_0 H_{\mathrm{DMI}}$ and the present analysis method is valid to extract the symmetric contribution in the creep regime. To determine $\mu_0 H_{\mathrm{DMI}}$, we need to measure R_{12} in the creep regime, however, it can be obtained from only a single $v - \mu_0 H_x$ curve in the flow region. However, in principle, the axes of the symmetric contribution in both creep and flow regimes are identical. Therefore, one can conclude that $\mu_0 H_{\mathrm{DMI}}$ can be determined for the flow regime as well as the creep regime based on the symmetric contribution. Hereafter, we will denote the determined $\mu_0 H_{\mathrm{DMI}}$ as $\mu_0 H^*_{\mathrm{DMI}}$.

Similarly, $v_0(\mu_0 H_x)$ can be determined by using the relation

$$v_0(\mu_0 H_x) = v_1(\mu_0 H_x)/[R_{12}(\mu_0 H_x)]^{\gamma}, \tag{2}$$

where $\gamma \equiv [\mu_0 H_{z1}]^{-1/4}/\{[\mu_0 H_{z1}]^{-1/4} - [\mu_0 H_{z2}]^{-1/4}\}$ and v_1 is the DW speed measured under $\mu_0 H_{z1}$. Figure 2(g) shows $v_0(\mu_0 H_x)$ determined with $\mu_0 H_{z1} = 2.1$ mT and $\mu_0 H_{z2} = 1.9$ mT. Though the data are slightly scattered since the statistical error in R_{12} is amplified greatly because of a large γ, the plot exhibits a noticeable variation in $v_0(\mu_0 H_x)$, as indicated by the solid line of the best linear fit. Such sizeable variation in $v_0(\mu_0 H_x)$ verifies that the antisymmetric contribution of the DW speed is mainly attributed to $v_0(\mu_0 H_x)$, since $\alpha(\mu_0 H_x)$ is solely responsible for the symmetric contribution. Such antisymmetric variation of $v_0(\mu_0 H_x)$ can be caused by several reasons, such as chiral damping [12,20], asymmetric DW width [21], or $\mu_0 H_x$-induced magnetization tilting inside the domains adjacent to the DWs. A detailed discussion about the antisymmetric contribution will be given later.

By use of $\mu_0 H^*_{\mathrm{DMI}}$, the antisymmetric contributions can be further analyzed. Figure 3(a) plots the asymmetry A of the DW speed with respect to ΔH_x (i.e., $\mu_0 \Delta H_x \equiv \mu_0 H_x + \mu_0 H^*_{\mathrm{DMI}}$)

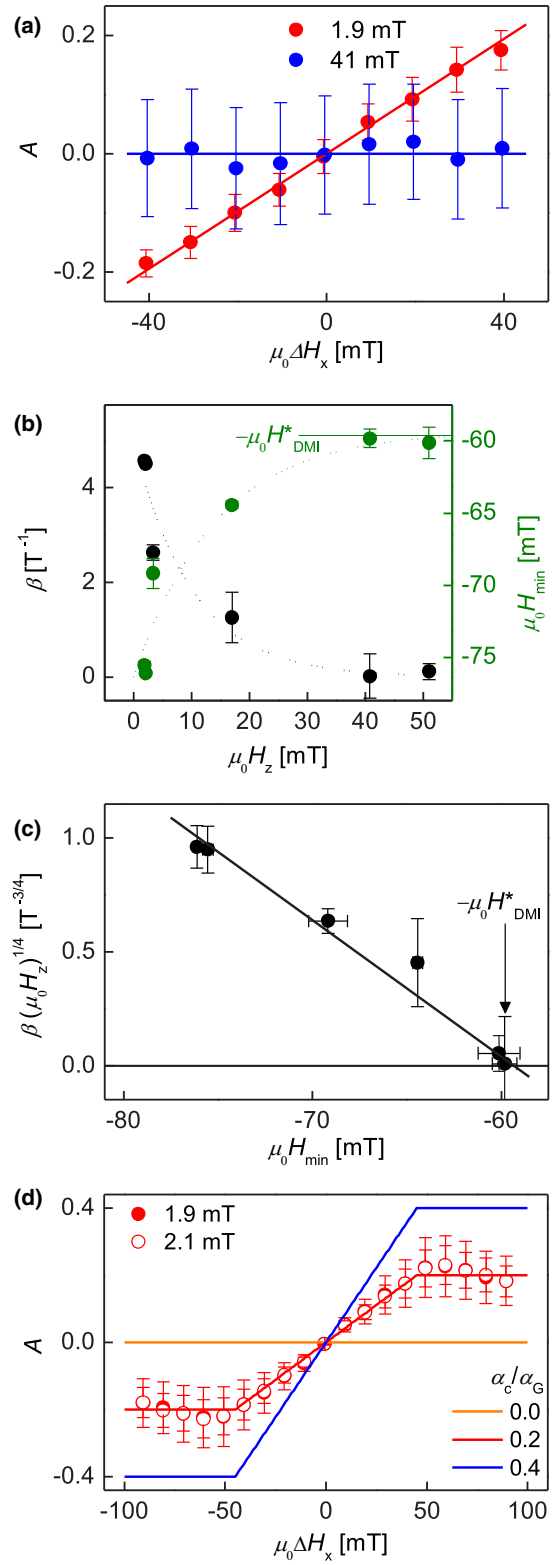

FIG. 3. Asymmetry of the DW speed over the creep and flow regimes. (a) Plot of A with respect to $\mu_0 \Delta H_x$ for the creep (red) and flow (blue) regimes. The solid lines show the best linear fit. (b) Plot of β (black) and $\mu_0 H_{\mathrm{min}}$ (green) with respect to $\mu_0 H_z$. The dotted lines indicate a simple exponential decay function. (c) Plot of $\beta[\mu_0 H_z]^{1/4}$ with respect to $\mu_0 H_{\mathrm{min}}$. The black solid line shows the best linear fit. (d) Plot of A with respect to $\mu_0 \Delta H_x$ for $\mu_0 H_z = 1.9$ and 2.1 mT. The solid lines show the prediction based on the chiral damping model.

for the creep (red) and flow (blue) regimes, where

$$A(\mu_0\Delta H_x) \equiv \frac{v(-\mu_0 H^*_{\rm DMI}+\mu_0\Delta H_x)-v(-\mu_0 H^*_{\rm DMI}-\mu_0\Delta H_x)}{v(-\mu_0 H^*_{\rm DMI}+\mu_0\Delta H_x)+v(-\mu_0 H^*_{\rm DMI}-\mu_0\Delta H_x)}. \quad (3)$$

It is clear from the figure that the creep regime exhibits a large asymmetry, in contrast with zero asymmetry in the flow regime. In the creep regime, one can readily derive the relation $A(\mu_0\Delta H_x) \cong \beta\mu_0\Delta H_x$ within the context of the creep criticality, where

$$\beta \equiv \frac{dv_0/d\mu_0\Delta H_x|_{\mu_0\Delta H_x=0}}{v_0(-\mu_0 H^*_{\rm DMI})}. \quad (4)$$

From the red symbols of Fig. 3(a), the value of β is determined as $4.6 \pm 0.1\,{\rm T}^{-1}$. The present value roughly matches the value ($=4.2 \pm 1.4\,{\rm T}^{-1}$) determined by the best linear fitting from Fig. 2(g). Even though the latter value has larger error bars due to the stochastic nature of the DW creep regime and the measurement with small $\mu_0 H_z$ difference, the conformity between the average values supports the validity of our approach.

Figure 3(b) summarizes the experimentally determined β (black) and $\mu_0 H_{\rm min}$ (green) with respect to $\mu_0 H_z$. It is evident from the figure that there exist sizeable asymmetries in the creep regime with a small $\mu_0 H_z$, but the asymmetry quickly decays as $\mu_0 H_z$ increases in the flow regime. Similarly, $\mu_0 H_{\rm min}$ approaches $-\mu_0 H^*_{\rm DMI}$ as $\mu_0 H_z$ increases. The dotted lines indicate a simple exponential decay function.

III. DISCUSSION

According to Ref. [10], $\alpha(\mu_0 H_x) = \alpha_0[\sigma_{\rm DW}(\mu_0 H_x)/\sigma_0]^{1/4}$, where $\sigma_{\rm DW}$ is the DW energy density, σ_0 is the Bloch-type DW energy density, and α_0 is a scaling constant. Recent studies [10,11,22] on the DMI effect on DWs have revealed that $\sigma_{\rm DW}(\mu_0 H_x)$ is given by

$$\sigma_{\rm DW}(\mu_0 H_x) = \begin{cases} \sigma_0 - 2\lambda K_{\rm D}\left|\frac{H_x+H^*_{\rm DMI}}{H_{\rm K}}\right|^2 & \text{for } |\mu_0 H_x+\mu_0 H^*_{\rm DMI}| \leqslant \mu_0 H_{\rm K} \\ \sigma_0 + 2\lambda K_{\rm D} - 4\lambda K_{\rm D}\left|\frac{H_x+H^*_{\rm DMI}}{H_{\rm K}}\right| & \text{otherwise} \end{cases}. \quad (5)$$

Here, $K_{\rm D}$ is the DW anisotropy energy density, λ is the DW width, and $\mu_0 H_{\rm K}$ ($\equiv 4K_{\rm D}/\pi M_{\rm S}$) is the DW anisotropy field, where the DW anisotropy energy is the difference between Bloch wall and Néel wall energy densities. The solid line in Fig. 2(f) is the best fit by these equations with the following best fitting parameters: $\alpha_0 = 3.81\,{\rm T}^{1/4}$, $\lambda K_{\rm D}/\sigma_0 = 0.027$, $\mu_0 H_{\rm K} = 29.7\,{\rm mT}$, and $\mu_0 H^*_{\rm DMI} = 59.3\,{\rm mT}$. For the case in which v_0 exhibits a finite asymmetry i.e., $v_0(-\mu_0 H^*_{\rm DMI}+\mu_0\Delta H_x) \cong v_0(-\mu_0 H^*_{\rm DMI}) + \beta\mu_0\Delta H_x$, one can again easily calculate that the apparent minimum $\mu_0 H_{\rm min}$ can be written as

$$\mu_0 H_{\rm min} \cong -\mu_0 H^*_{\rm DMI} - \eta\beta[\mu_0 H_z]^{1/4}, \quad (6)$$

where $\eta \equiv \sigma_0[\mu_0 H_{\rm K}]^2/\alpha_0\lambda K_{\rm D}$. The prediction given by Eq. (6) is experimentally confirmed as observed by the linear relation between $\beta[\mu_0 H_z]^{1/4}$ and $\mu_0 H_{\rm min}$ in Fig. 3(c). Therefore, one can conclude that the asymmetry is the origin of the deviation in $\mu_0 H_{\rm min}$ and therefore, $\mu_0 H_{\rm min}$ converges to $-\mu_0 H^*_{\rm DMI}$ as the asymmetry vanishes in the flow regime.

To extend our understanding on the antisymmetric contribution, we further analyze the nature of A in the creep regime. Figure 3(d) plots A with respect to $\mu_0\Delta H_x$ at $\mu_0 H_z = 1.9$ and 2.1 mT. It is clear from figure that A is saturated as a large $\mu_0\Delta H_x$ with a transition region in between. The present dependence of A on $\mu_0\Delta H_x$ resembles the typical dependence of the spin-orbit torque [23], which is known to follow the DW chirality. As one of the possible scenarios, the chiral damping model [12,20] is adopted to explain the typical dependence of $\mu_0\Delta H_x$. The solid lines in the figure are the prediction from the chiral damping model with different values of $\alpha_{\rm c}/\alpha_{\rm G}$, 0 (orange), 0.2 (red), and 0.4 (blue), based on the relation $A \cong \alpha_{\rm c}/\alpha_{\rm G}\cos\psi$ where $\alpha_{\rm c}$ is the chiral damping constant, α_G is the Gilbert damping constant, and ψ is the angle of the magnetization inside the DW [24]. The value $\alpha_{\rm c}/\alpha_{\rm G} = 0.2$ better fits the experimental data. Though the present analysis supports that A is attributed to the DW chirality, it requires further deliberate experiment and theoretical support to extract the exact portion of the chiral damping mechanism out of all the other possible chiral mechanisms.

The DW motion in the flow regime can be described by the one-dimensional DW model [25,26] based on the Landau-Lifshitz-Gilbert equation [27]. It is well known that, under a $\mu_0 H_z$ larger than the Walker breakdown field [28], the DW exhibits precessional motion [29]. By solving the one-dimensional DW model, the DW speed is given by $v = \lambda(\gamma_0\mu_0 H_z - 2\pi/T)/\alpha_G$, where γ_0 is the gyromagnetic ratio. The precession period T is then written as

$$T = \frac{1+\alpha_{\rm G}^2}{\gamma_0}\int_0^{2\pi}\frac{d\psi}{\mu_0 H_z - \alpha_G\frac{\pi}{2}\mu_0(H_x+H_{\rm DMI})\sin\psi + \alpha_G\frac{\pi}{2}\mu_0 H_{\rm K}\sin\psi\cos\psi}, \quad (7)$$

where ψ is the angle of the magnetization inside the DW. Since $\mu_0 H_z \gg \alpha_G\mu_0 H_{\rm K}$ for the experimental condition in the flow regime with a small α_G, it is a good approximation to write T

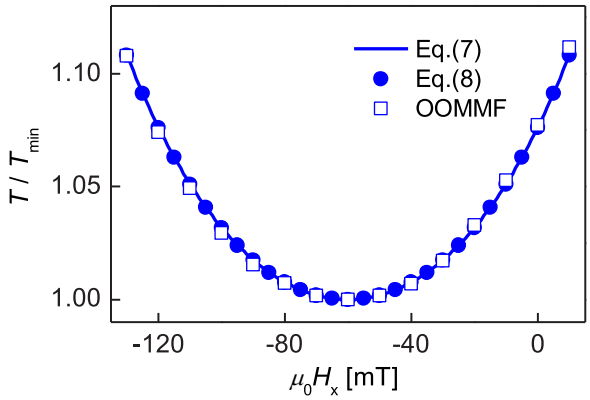

FIG. 4. Plot of $T/T_{\rm min}$ with respect to $\mu_0 H_x$, calculated by Eq. (7) (solid line) and Eq. (8) (circular symbols) as well as by micromagnetic simulation (square symbols) at $\mu_0 H_z = 51$ mT.

as

$$T \approx \frac{1+\alpha_{\rm G}^2}{\gamma_0}\int_0^{2\pi}\frac{d\psi}{\mu_0 H_z - \alpha_G\frac{\pi}{2}\mu_0(H_x+H_{\rm DMI})\sin\psi} = \frac{1+\alpha_{\rm G}^2}{\gamma_0}\frac{2\pi}{\sqrt{(\mu_0 H_z)^2-\alpha_{\rm G}^2\left(\frac{\pi}{2}\right)^2(\mu_0 H_x+\mu_0 H_{\rm DMI})^2}}. \quad (8)$$

Figure 4 plots the numerical evaluation $T/T_{\rm min}$ of Eqs. (7) and (8) for our experimental condition, where $T_{\rm min}$ is defined as T at $\mu_0 H_x = -\mu_0 H_{\rm DMI}$. The micromagnetic simulation results by use of the object oriented micromagnetic framework are plotted together. The figure clearly shows that all results match each other with accuracy better than 1%. Therefore, it is good to write v as

$$v \approx \frac{\lambda\gamma_0}{\alpha_{\rm G}}\left(\mu_0 H_z - \frac{1}{1+\alpha_{\rm G}^2}\sqrt{(\mu_0 H_z)^2-\alpha_{\rm G}^2\left(\frac{\pi}{2}\right)^2(\mu_0 H_x+\mu_0 H_{\rm DMI})^2}\right) \approx \frac{\lambda\gamma_0\alpha_{\rm G}}{1+\alpha_{\rm G}^2}\mu_0 H_z\left(1+\left(\frac{\pi}{2}\right)^2\frac{(\mu_0 H_x+\mu_0 H_{\rm DMI})^2}{2(\mu_0 H_z)^2}\right), \quad (9)$$

which exhibits symmetric behavior with a parabolic dependence on $\mu_0 H_x + \mu_0 H_{\rm DMI}$. Note that the parabolic variation originates from the suppression of precessional DW motion because of the additional energy barrier enhanced by an in-plane magnetic field [9]. It is also worth noting that λ also varies with respect to $\mu_0 H_x$ [21], but the variation of λ is expected to be less than a few tens of percent. Therefore, the large variation of v observed in Fig. 2(e) is mostly attributed to the suppression of the precessional DW motion rather than the λ variation.

IV. CONCLUSION

In conclusion, we examine the nature of the asymmetric behavior in DW motion over the creep and flow regimes. Based on the distinct dependence of the DW speed on the in-plane and out-of-plane magnetic fields, the symmetric and antisymmetric contributions of the DW speed are decomposed, enabling one to quantify the pure effect of the DMI. The results show that the antisymmetric contribution vanishes gradually across the regimes, while the symmetric contribution remains unchanged, confirming the fundamental quantity of the DMI-induced magnetic field across the regimes. The present observation elucidates the underlying physics on the recent puzzling issue in the DMI-related chiral DW dynamics.

ACKNOWLEDGMENTS

This work was supported by the Samsung Science & Technology Foundation (SSTF-BA1802-07) and the National Research Foundations of Korea (NRF) funded by the Ministry of Science, ICT (MSIT) (2015M3D1A1070465). D.-H.K. was supported by a grant funded by the Korean Magnetics Society and from Overseas researcher under the Postdoctoral Fellowship of Japan Society for the Promotion of Science (Grant No. P16314). B.-C.M. was supported by the KIST institutional program and the National Research Council of Science & Technology (NST) Grant No. CAP-16-01-KIST.

D.-H.K. planned and designed the experiment and S.-B.C. supervised the study. D.-H.K. and D.-Y.K. carried out the measurement. S.-C.Y. and B.-C.M. prepared the samples. D.-H.K. and S.-B.C. performed the analysis and wrote the manuscript. All authors discussed the results and commented on the manuscript.

The authors declare no competing financial interests.

[1] I. E. Dzialoshinskii, Zh. Eksp. Teor. Fiz. **32**, 1547 (1957) [Sov. Phys. JETP **5**, 1259 (1957)].
[2] T. Moriya, Phys. Rev. **120**, 91 (1960).
[3] G. Chen, J. Zhu, A. Quesada, J. Li, A. T. N'Diaye, Y. Huo, T. P. Ma, Y. Chen, H. Y. Kwon, C. Won, Z. Q. Qiu, A. K. Schmid, and Y. Z. Wu, Phys. Rev. Lett. **110**, 177204 (2013).
[4] K.-S. Ryu, L. Thomas, S.-H. Yang, and S. Parkin, Nat. Nanotechnol. **8**, 527 (2013).
[5] P. P. J. Haazen, E. Murè, J. H. Franken, R. Lavrijsen, H. J. M. Swagten, and B. Koopmans, Nat. Mater. **12**, 299 (2013).
[6] S. Emori, U. Bauer, S.-M. Ahn, E. Martinez, and G. S. D. Beach, Nat. Mater. **12**, 611 (2013).
[7] S.-H. Yang, K.-S. Ryu, and S. Parkin, Nat. Nanotechnol. **10**, 221 (2015).
[8] K.-W. Moon, D.-H. Kim, S.-C. Yoo, S.-G. Je, B. S. Chun, W. Kim, B.-C. Min, C. Hwang, and S.-B. Choe, Sci. Rep. **5**, 9166 (2015).
[9] A. Thiaville, S. Rohart, É. Jué, V. Cros, and A. Fert, Europhys. Lett. **100**, 57002 (2012).
[10] S.-G. Je, D.-H. Kim, S.-C. Yoo, B.-C. Min, K.-J. Lee, and S.-B. Choe, Phys. Rev. B **88**, 214401 (2013).

[11] A. Hrabec, N. A. Porter, A. Wells, M. J. Benitez, G. Burnell, S. McVitie, D. McGrouther, T. A. Moore, and C. H. Marrows, Phys. Rev. B **90**, 020402(R) (2014).
[12] E. Jué, C. K. Safeer, M. Drouard, A. Lopez, P. Balint, L. Buda-Prejbeanu, O. Boulle, S. Auffret, A. Schuhl, A. Manchon, I. M. Miron, and G. Gaudin, Nat. Mater. **15**, 272 (2016).
[13] M. Vaňatka, J.-C. Rojas-Sánchez, J. Vogel, M. Bonfim, M. Belmeguenai, Y. Roussigné, A. Stashkevich, A. Thiaville, and S. Pizzini, J. Phys.: Condens. Matter **27**, 326002 (2015).
[14] Y. Yoshimura, K.-J. Kim, T. Taniguchi, T. Tono, K. Ueda, R. Hiramatsu, T. Moriyama, K. Yamada, Y. Nakatani, and T. Ono, Nat. Phys. **12**, 157 (2016).
[15] D.-H. Kim, S.-C. Yoo, D.-Y. Kim, K.-W. Moon, S.-G. Je, C.-G. Cho, B.-C. Min, and S.-B. Choe, Appl. Phys. Lett. **104**, 142410 (2014).
[16] K.-J. Kim, J.-C. Lee, S.-M. Ahn, K.-S. Lee, C.-W. Lee, Y. J. Cho, S. Seo, K.-H. Shin, S.-B. Choe, and H.-W. Lee, Nature (London) **458**, 740 (2009).
[17] P. J. Metaxas, J. P. Jamet, A. Mougin, M. Cormier, J. Ferré, V. Baltz, B. Rodmacq, B. Dieny, and R. L. Stamps, Phys. Rev. Lett. **99**, 217208 (2007).
[18] S. Lemerle, J. Ferré, C. Chappert, V. Mathet, T. Giamarchi, and P. Le Doussal, Phys. Rev. Lett. **80**, 849 (1998).
[19] D.-Y. Kim, D.-H. Kim, J. Moon, and S.-B. Choe, Appl. Phys. Lett. **106**, 262403 (2015).
[20] C. A. Akosa, I. M. Miron, G. Gaudin, and A. Manchon, Phys. Rev. B **93**, 214429 (2016).
[21] D.-Y. Kim, D.-H. Kim, and S.-B. Choe, Appl. Phys. Express **9**, 053001 (2016).
[22] D.-H. Kim, S.-C. Yoo, D.-Y. Kim, B.-C. Min, and S.-B. Choe, Sci. Rep. **7**, 45498 (2017).
[23] D.-Y. Kim, M.-H. Park, Y.-K. Park, J.-S. Kim, Y.-S. Nam, D.-H. Kim, S.-G. Je, B.-C. Min, and S.-B. Choe, NPG Asia Mater. **10**, e464 (2018).
[24] See Supplemental Material at http://link.aps.org/supplemental/10.1103/PhysRevB.99.134401 for derivation of the anti-symmetric contribution A based on the chiral damping model, see Refs. [30–35].
[25] J. C. Slonczewski, in *Magnetism and Magnetic Materials — 1971 Parts 1 and 2*, edited by C. D. Graham and J. J. Rhyne, AIP Conf. Proc. No. 5 (AIP, New York, 1972), p. 170.
[26] B. Hillebrands and A. Thiaville, Top. Appl. Phys. **101**, 161 (2006).
[27] T. L. Gilbert, IEEE Trans. Magn. **40**, 3443 (2004).
[28] G. S. D. Beach, C. Nistor, C. Knutson, M. Tsoi, and J. L. Erskine, Nat. Mater. **4**, 741 (2005).
[29] M. Hayashi, L. Thomas, C. Rettner, R. Moriya, and S. S. P. Parkin, Nat. Phys. **3**, 21 (2007).
[30] D.-H. Kim, K.-W. Moon, S.-C. Yoo, B.-C. Min, K.-H. Shin, and S.-B. Choe, IEEE Trans. Magn. **49**, 3207 (2013).
[31] A. Thiaville, Y. Nakatani, J. Miltat, and Y. Suzuki, Europhys. Lett. **69**, 990 (2005).
[32] S. Rohart and A. Thiaville, Phys. Rev. B **88**, 184422 (2013).
[33] S. Mizukami, E. P. Sajitha, D. Watanabe, F. Wu, T. Miyazaki, H. Naganuma, M. Oogane, and Y. Ando, Appl. Phys. Lett. **96**, 152502 (2010).
[34] S.-G. Je, S.-C. Yoo, J.-S. Kim, Y.-K. Park, M.-H. Park, J. Moon, B.-C. Min, and S.-B. Choe, Phys. Rev. Lett. **118**, 167205 (2017).
[35] S.-J. Yun, J.-C. Lee, and S.-B. Choe, J. Korean Magn. Soc. **21**, 204 (2011).